

## Arbitrarily Configurable Nonlinear Topological Modes

Kai Bai,<sup>1</sup> Jia-Zheng Li<sup>1</sup>,<sup>✉</sup> Tian-Rui Liu,<sup>1</sup> Liang Fang,<sup>1</sup> Duanduan Wan,<sup>1,\*</sup> and Meng Xiao<sup>1,2,†</sup>

<sup>1</sup>Key Laboratory of Artificial Micro- and Nano-structures of Ministry of Education and School of Physics and Technology, Wuhan University, Wuhan 430072, China

<sup>2</sup>Wuhan Institute of Quantum Technology, Wuhan 430206, China

 (Received 14 December 2023; revised 14 April 2024; accepted 8 August 2024; published 12 September 2024)

Topological modes (TMs) are typically localized at boundaries, interfaces and dislocations, and exponentially decay into the bulk of a large enough lattice. Recently, the non-Hermitian skin effect has been leveraged to delocalize the wave functions of TMs from the boundary and thus to increase the capacity of TMs dramatically. Here, we explore the capability of nonlinearity in designing and configuring the wave functions of TMs. With growing intensity, wave functions of these in-gap nonlinear TMs undergo an initial deviation from exponential decay, gradually merge into arbitrarily designable plateaus, then encompass the entire nonlinear domain, and eventually concentrate at the nonlinear boundary. Intriguingly, such extended nonlinear TMs are still robust against defects and disorders, and stable in dynamics under external excitation. Advancing the conceptual understanding of the nonlinear TMs, our results open new avenues for increasing the capacity of TMs and developing compact and configurable topological devices.

DOI: [10.1103/PhysRevLett.133.116602](https://doi.org/10.1103/PhysRevLett.133.116602)

*Introduction*—The concept of topological matters flourished rapidly in various fields such as condensed matters [1], photonics [2–9], circuits [10–13], and acoustic and mechanical systems [14–19]. As ensured by the conventional bulk-boundary correspondence [20], topologically nontrivial bulks give rise to topological modes (TMs) localized at the boundary, interface, and crystallographic defects such as dislocations and disclinations [21]. These TMs are robust against disorders and backscattering immunity to certain defects. Numerous novel phenomena and potential applications rooted in TMs have been elucidated in the past decades [22–29]. However, as inherited from the bulk-boundary correspondence, TMs exponentially decay into the bulk and hence have limited capacity. The requirement of bulky topological materials and the limited available capacity of TMs exhibit a bottleneck in potential applications. Recently, the non-Hermitian skin effect [30–32] and imaginary gauge field [33,34] have been leveraged to delocalize TMs [17,35–37]. Therein, the nonreciprocal coupling tunes the TMs into completely extended modes. Here, we explore the consequence of nonlinearity in configuring TMs. Our Letter demonstrates the capability of harnessing nonlinearity to reshape TMs into arbitrarily designed profiles such as square, isosceles triangular, and sinusoidal waves. In addition, instead of a fixed mode profile for each sample in previous works [17,35], the lattices covered by the extended TMs herein can be easily tuned with the input intensity.

Nonlinearity is ubiquitous [38–45], which, coupled with topology, can lead to exciting physics and novel phenomena [46–49]. The topological edge [46,47] and bulk solitons [48,49] were discovered in nonlinear topological insulators. They are strongly self-localized and propagate unidirectionally along the edge or inside the bulk when the nonlinear effects compensate for the dispersion. Thanks to the inherent configurability of nonlinear structures, the excitation intensity can induce topological phase transitions, leading to the emergence of topologically robust edge states [50–52] and corner states [53,54]. Recently, nonlinear effects have been extended to non-Hermitian topological insulators for active tuning of parity-time symmetry and the corresponding topological edge states [55,56]. These nonlinear topologies span diverse systems of physics, ranging from quantum electronics and photonics to classical systems such as acoustics and circuits. The dependence of TMs on the excitation intensity paves the way for configurable devices imbued with topological features. However, previous works still focus on localized modes, which have limited capacity. Consequently, any related applications must be built upon a bulk lattice, making them bulky in footprint and costly to fabricate. It is natural to ask: Can nonlinearities be utilized to design and configure TMs? Clearly, it would be of great interest to pursue arbitrarily configurable nonlinear TMs which are robust against disorders as protected by a nontrivial topology while uniquely controllable through external sources as inherited from the configurability of nonlinearity. Exploring nonlinear topological physics continues to be an intriguing frontier yet to be fully unveiled.

\*Contact author: [ddwan@whu.edu.cn](mailto:ddwan@whu.edu.cn)

†Contact author: [pmtxiao@whu.edu.cn](mailto:pmtxiao@whu.edu.cn)

Here, we leverage nonlinearity to deform, reshape, and design the wave functions of TMs. Our system consists of a one-dimensional lattice that is linear and topologically nontrivial and a nonlinear one that features alternating linear and nonlinear couplings [50–53]. In the low-intensity regime (where the nonlinearity is negligible), the nonlinear chain remains topologically trivial, supporting a topological zero mode (TZM) localized at the interface. With increasing intensity, the profile of the TZM is deformed on the nonlinear lattice and deviates from the exponential decaying behavior. As the intensity is above a certain threshold, the TZM merges into an arbitrarily designable plateau that gradually covers the entire nonlinear lattice domain. Interestingly, the eigenfrequencies of TZMs stay at the gap center of the nonlinear eigenfrequency spectrum. Since the local nonlinearities drastically alter the periodicity of Hamiltonians, the nonlinear topological properties cannot be simply characterized based on the band topology defined in linear systems. In addition, an arbitrarily configurable TZM will certainly violate the traditional bulk-boundary correspondence, as the nonlinear TZMs are no longer orthogonal to the bulk modes (nor biorthogonal if considering non-Hermitian systems). To properly characterize the topological origin of the TZMs, we employ the nonlinear spectral localizer [57–59], which makes use of the system’s real-space description and yields local invariants that are protected by local gaps. When excited, TZMs are stable in dynamics against noise while tunable with the excitation power. Our findings promote the understanding of configurable TZMs and open new avenues for utilizing the configurability in quantum and classical nonlinear systems.

*Shape shifting of TZMs with nonlinearity*—Our system consists of a nonlinear Su-Schrieffer-Heeger (NL-SSH) chain [50] and a linear one [60] as sketched in Fig. 1(a). The nonlinear Schrödinger equation in real space is

$$H_{|\psi\rangle}|\psi\rangle = \omega|\psi\rangle, \quad (1)$$

where  $\omega$  is the eigenfrequency.  $|\psi\rangle \equiv (\dots, a_i, b_i, \dots)^T$  is the eigenstate with superscript  $T$  short for transpose, and  $a_i, b_i$  representing the field amplitudes at different sublattices of the  $i$ th unit cell. The tight-binding Hamiltonian  $H_{|\psi\rangle}$  is

$$H_{|\psi\rangle} = \sum_{i < n} (\nu_i |a_i\rangle \langle b_i| + \kappa_{i-1} |a_i\rangle \langle b_{i-1}|) + \kappa_d |a_{n+1}\rangle \langle b_n| + \sum_{i > n} (t |a_i\rangle \langle b_i| + \tau |a_{i+1}\rangle \langle b_i|) + \text{H.c.}, \quad (2)$$

The nonlinear chain has  $n$  unit cells, and  $\nu_i$  and  $\kappa_i$  represent the corresponding intracell and intercell couplings, respectively.  $\kappa_i = \tilde{\kappa}_i + \alpha(|a_{i+1}|^2 + |b_i|^2)$  with a linear term  $\tilde{\kappa}_i$  and a Kerr nonlinear coefficient  $\alpha$  [50–54].  $t$  and  $\tau$  denote the intracell and intercell coupling in the linear chain, respectively.  $\kappa_d$  is the coupling at the interface. Given the specific

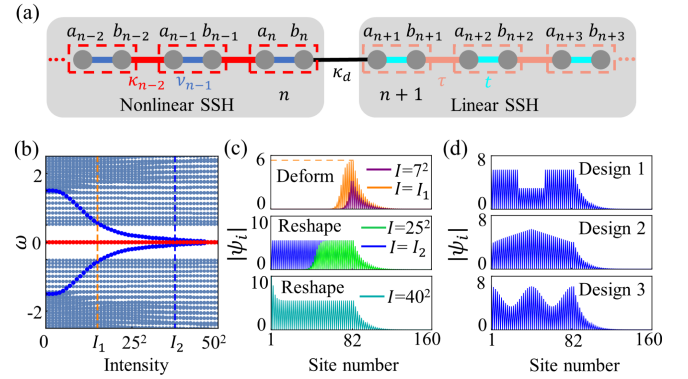


FIG. 1. (a) Schematic of a tight-binding lattice consisting of a nonlinear (left) and linear (right) SSH chain.  $a_i$  and  $b_i$  are the field amplitudes at different sites of the  $i$ -th unit cell (marked by the dashed boxes). The red bonds denote nonlinear intercell couplings  $\{\kappa_{i-1}(b_{i-1}, a_i)\}$  that depend on the intensities of sites connected by the bonds. All the other couplings are linear with the hoppings being  $\{\nu_i\}$ ,  $\kappa_d$ ,  $t$  and  $\tau$  for the blue, black, cyan and pink bonds, respectively. (b) Evolution of the nonlinear eigenfrequency spectrum of a finite lattice as the intensity  $I$  is increased. The red dots mark the TZM, whose eigenfrequency is pinned at zero independent of  $I$ . (c) The wave functions of the TZM for different  $I$ . At  $I_1 = 15^2$ , the wave function emerges a plateau. The orange horizontal dashed line is for eye guiding. This plateau will gradually extend to the entire nonlinear domain at  $I_2 = 36.5^2$  and eventually the field concentrates at the nonlinear boundary. (d) Based on Eq. (6), the shape of the plateau (at the corresponding  $I_2$ ) can be turned into an arbitrary shape, such as a square, isosceles triangle, cosine, etc. The parameters used are  $t = 2$ ,  $\tau = \kappa_d = 2.5$ ,  $\{\nu_i\} = 2.5$ ,  $\kappa_i = \tilde{\kappa}_i + \alpha(|a_i|^2 + |b_{i-1}|^2)$  with  $\alpha = 0.05$ .  $n = 41$  and the total number of lattice sites is 161. In (b) and (c),  $\tilde{\kappa}_i = 1$ . In (d), the corresponding distribution of  $\tilde{\kappa}_i$  are provided in the Supplemental Material, Sec. 2 [61].

form of nonlinearity, the eigenvalues and eigenstates of the nonlinear Schrödinger equation can be solved numerically using a self-consistent method [54]. Figure 1(b) shows the eigenvalue distribution versus the total wave function intensity  $I = \langle \psi | \psi \rangle = \sum_i (|a_i|^2 + |b_i|^2)$ . The red dots mark the states with zero eigenfrequencies inside the gap. There are another two modes (dark blue dots) that gradually merge into the gap and approach the zero frequency. These two modes originate from the bulk modes inside the nonlinear lattice region, the evolution of the nonlinear part of these wave functions is similar to the topological edge states introduced through nonlinearity-induced topological transitions [50,51] (See detailed discussion in the Supplemental Material, Sec. 1 [61]).

When  $I$  is small (the nonlinear effects are negligible), the NL-SSH remains topologically trivial ( $\nu_i > \tilde{\kappa}_i$ ), and forms an interface with the topologically nontrivial linear SSH ( $\tau > t$ ). Therefore, there is a TZM localized at the interface and exponentially decaying toward the chains on both sides. With the increasing of  $I$ , the wave function of the TZM deviates from exponential decay on the nonlinear

lattice [see Fig. 1(c), at  $I = 7^2$ , for example]. Subsequently, the wave function exhibits a plateau at  $I = I_1$  [the orange solid line in Fig. 1(c)], and the orange dashed line indicates the plateau. This plateau then gradually extends to cover the whole nonlinear lattice domain when  $I > I_1$  [see Fig. 1(c), the green line at  $I = 25^2$ , for example], and eventually fills the entire NL-SSH chain at  $I = I_2$  [the blue line in Fig. 1(c)]. When  $I$  is further increased to be above  $I_2$ , the wave function will concentrate at the left boundary of the nonlinear lattice while the plateau built before is preserved [see Fig. 1(c), the cyan line at  $I = 40^2$ , for example]. Interestingly, the plateau can be designed arbitrarily. Similar to Fig. 1(c), the wave function of the TZM starts with an interface state and gradually extends to cover the whole nonlinear lattice under the increasing of  $I$ . Figure 1(d) shows three different profiles, square, isosceles triangle, and cosine, of the TZMs at their corresponding critical intensity  $I = I_2$ . Furthermore, the magnitude at the linear part of the wavefunction of the TZM is tunable with  $\kappa_d$  (Details provided in the Supplemental Material, Sec. 2 [61]).

*Topological protection of the TZMs*—Generally, nonlinear effects are intrinsically local. When the nonlinear effects are strong, the spatial periodicity of  $H_{|\psi\rangle}$  will be broken [see Fig. 2(a)], and the conventional topological invariant defined in the momentum space becomes ill defined. Recently, the notions of local topological markers have been introduced to address situations where translation symmetry is absent, such as open boundaries, disorder, and nonlinearity [57,58,77–79]. Here we adopt a nonlinear spectral localizer [57,58] to characterize the topological origin of the TZMs (see the Supplemental Material, Sec. 3 [61]). The spectral localizer is a Hermitian composite operator  $L_\lambda$  that combines  $H_{|\psi\rangle}$  with the information of the real-space position operators  $X$  using a nontrivial Clifford representation,

$$L_{\lambda \equiv (x, \tilde{\omega})}(X, H_{|\psi\rangle}) = \beta(X - x\mathbf{I}) \otimes \Gamma_x + (H_{|\psi\rangle} - \tilde{\omega}) \otimes \Gamma_y. \quad (3)$$

Here,  $\Gamma_x$  and  $\Gamma_y$  are a Pauli matrices,  $\mathbf{I}$  is the identity matrix,  $\beta$  is a hyperparameter to ensure that the units are comparable,  $X \equiv x_i$  where  $x_i$  denotes the coordinate of the  $i$ th lattice site. Based on the chiral symmetry, the spectral localizer can be written in a reduced form as  $\tilde{L}_{\lambda \equiv (x, \tilde{\omega})} = \beta(X - x\mathbf{I})\Pi + H - i\tilde{\omega}\Pi$  with  $\Pi$  being the system's chiral operator. At a specified location  $x$  and frequency  $\tilde{\omega}$  [marked as  $\lambda \equiv (x, \tilde{\omega})$ , which can be any value, even outside of the system's spatial and spectral regions], the local topological invariant is given by

$$C_\lambda = \frac{1}{2} \text{sig}(L_\lambda), \quad (4)$$

where sig is the signature of a matrix, i.e., its number of the positive eigenvalues minus that of the negative ones. For

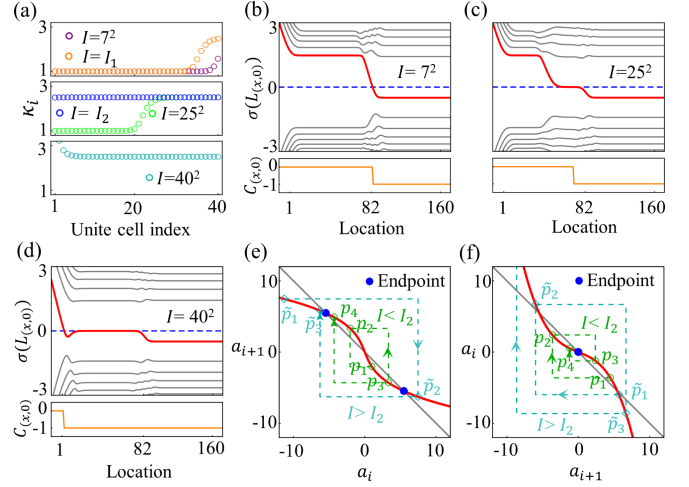


FIG. 2. (a) The distribution of  $\{\kappa_i\}$  of the TZMs for different  $I$ . (b)–(d) Eigenvalues of the spectral localizer  $\sigma(L_\lambda)$  and the topological invariant  $C_\lambda$  versus the location  $x$  for different  $I$ , where the solid red lines correspond to the smallest singular value  $\mu_\lambda$ , i.e., the eigenvalue closest to zero. When  $\mu_\lambda \approx 0$ , the system supports a state near  $\lambda$ . Thus, the solid red lines can also be used to approximately predict the width of the plateau. (e), (f) The schematic of iterative trajectories of  $\{a_i\}$  as the site number increases (e) or decreases (f). The red lines are given by Eq. (6) and the gray lines correspond to  $a_i = -a_{i+1}$ . The dark green and cyan dashed lines indicate two iteration trajectories corresponding to  $I < I_2$  and  $I > I_2$ . In (b)–(d),  $\beta = 0.2$ , and the lattice constant and energy (frequency) unit are set as 1. Other parameters are the same as those in Fig. 1(c).

different  $I$ , Figs. 2(b)–2(d) show the eigenvalues of  $L_\lambda$  [denoted as  $\sigma(L_\lambda)$ ] and the corresponding  $C_\lambda$  at  $\tilde{\omega} = 0$ . It is clear that both  $\sigma(L_\lambda)$  and  $C_\lambda$  are intensity dependent.  $C_\lambda$  changes when one of  $\sigma(L_\lambda)$  crosses zero such as the red line in the upper panel of Figs. 2(b)–2(d). When the red line crosses zero at  $x_0$  [ $\det(L_\lambda) = 0$ ], the system exhibits a state approximately localized at  $\lambda = (x_0, 0)$ , thus realizing the bulk-boundary correspondence, i.e., the change of  $C_\lambda$  corresponds to a TZM. The smallest singular value  $\mu_\lambda = \min[|\sigma(L_\lambda)|]$  of the spectral localizer provides additional information of the system at  $\lambda$ . Small values of  $\mu_\lambda$  allow the existence of a state approximately localized near  $\lambda$ , while large ones indicate that the system does not support such a state. Therefore,  $\mu_\lambda$  can be thought of as a “local band gap,” and the topological protection of the TZMs can be characterized by

$$\|\Delta H(\delta)\| \leq \mu_\lambda^{\max}, \quad (5)$$

where  $\|\Delta H(\delta)\|$  is the largest singular value of  $\Delta H(\delta) = H_{|\psi\rangle}(\delta) - H_{|\psi\rangle}$ , with  $H_{|\psi\rangle}(\delta)$  representing the perturbed nonlinear Hamiltonian. Let  $\mu_\lambda^{\max} \equiv \max_x [\mu_{(x,0)}(X, H_{|\psi\rangle})]$  denotes the maximum  $\mu_{(x,0)}$  inside the topological domain ( $C_\lambda \neq 0$ ). As long as Eq. (5) is satisfied, the topological protection guarantees the

existence of a TZM with a similar wave function (see the Supplemental Material, Sec. 4 [61]). Here, nonlinearity does not create or annihilate TZMs, but it can change the profiles of the TZMs.

The eigenstates of the TZM in the nonlinear part satisfy

$$\nu_i a_i + (\tilde{\kappa}_i + \alpha a_{i+1}^2) a_{i+1} = 0, \quad (6)$$

and all  $b_i = 0$  due to the bipartite property. Figure 2(e) sketches the iterative trajectories of  $\{a_i\}$  for two different paths as the site number increases. Regardless of whether the starting point has a smaller amplitude (such as  $p_1$ , corresponding to  $I < I_2$ ) or a larger amplitude (such as  $\tilde{p}_1$ , corresponding to  $I > I_2$ ), it will eventually converge to endpoints with a nonzero amplitude value, marked by the blue dots. Here, the two blue points correspond to the plateau in Fig. 1(c), and the corresponding height of the platform is

$$|a_i| = \sqrt{(\nu_i - \{\tilde{\kappa}_i\})/\alpha}. \quad (7)$$

The intensity  $I$  as well as the coefficients  $\{\nu_i\}$ ,  $\{\tilde{\kappa}_i\}$  and  $\alpha$  affect how fast the iteration converges and thus the width of the plateau. Figure 2(f) shows the iterative trajectories of  $\{a_i\}$  along the direction of decreasing the site number. Amplitudes starting at less than the plateau (such as  $p_1$ , corresponding to  $I < I_2$ ) converge to the endpoint with vanishing amplitude, which corresponds to the decaying of  $\{a_i\}$  towards the left boundary of the NL-SSH chain. While amplitudes starting at larger than the plateau (such as  $\tilde{p}_1$ , corresponding to  $I > I_2$ ) will diverge at the left boundary, and the  $I = 40^2$  curve in Fig. 1(c) is one such case. The waveform of TZM in the linear chain can be handled similarly, and the magnitude is tunable with  $\kappa_d$  through  $a_n \nu_n + a_{n+1} \kappa_d = 0$  (see details in the Supplemental Material, Sec. 2 [61]). Furthermore, when we vary  $\tilde{\kappa}_i$ , the shape of the plateau can be designed arbitrarily based on Eq. (6) [see Fig. 1(d) and the Supplemental Material, Sec. 5 [61] for a systematic approach.]

*Stability of the TZMs under external excitation—* Compared with conventional linear topological structures, nonlinear ones exhibit inherent configurability. In particular, the dynamics of TZMs depend on the intensity, which offers a unique controllability utilizing external sources. However, it still remains a fundamental challenge to reach the designed TZMs in practical use. First, the nonlinear TZM depends delicately on the local field distributions. Second, the excited state in general is a composition of different modes of the corresponding Green's function, and such a composition typically deviates from the TZM. Third, one needs to exert additional effort to stabilize the excited mode. Here as sketched in Fig. 3(a), we introduce external sources (yellow spots) and losses (unavoidable in nature) at different sites to obtain stable excited states that are almost identical to TZMs. The dynamics in the time-domain

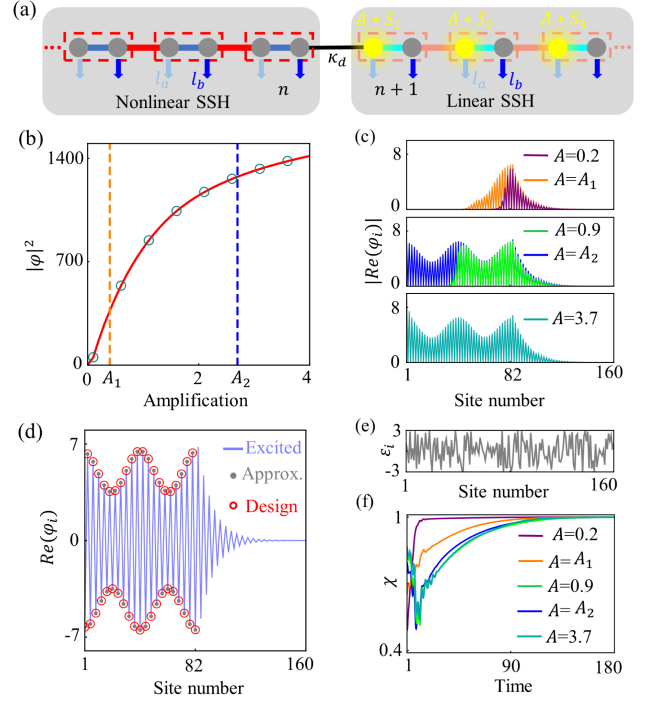


FIG. 3. (a) Schematic of excitation. These yellow spots represent the locations of the sources, all of which are located in the linear chain, and the number of excitation sources can be reduced to one. The corresponding distribution is  $\{A * S_i\}$  where  $A$  denotes a global amplification factor.  $l_a$  and  $l_b$  are the losses at different sites, which is unavoidable in real systems and can be used to stabilize the excited state. (b) The intensity  $|\phi|^2$  of the excited state versus  $A$ , where  $A_1 = 0.4$  and  $A_2 = 2.7$ . The dark cyan circles obtained from Eq. (8) coincide with the solid red line solved using the self-consistent Green's function [Eq. (S8)]. (c) The wave functions at different  $A$ . (d) The excited wave-function (light blue line) is almost perfectly consistent with the results from Eq. (9) (gray dots, the approximate wave function) and Eq. (6) (red circles, the wave function of targeted TZM). (e) A typical distribution of noise. (f) Evolution of the similarity function  $\chi$  for different  $A$ . In the presence of noise,  $\chi$  deviates from 1 and will fall back to 1 eventually. Thus, we can obtain stable excited states almost identical to TZMs. Here,  $\tilde{\omega} = 0$ ,  $l_a = 0.01$  and  $l_b = 0.5$ , and the distribution of  $\{S_i\}$  is provided in Fig. S6(b). Other parameters are the same as those in design 3 of Fig. 1(d).

through external excitation can be captured by

$$\frac{\partial}{\partial t} |\phi\rangle = -i(H_{|\phi\rangle} + H_0)|\phi\rangle + A|S\rangle e^{-i\tilde{\omega}t}, \quad (8)$$

where  $H_0 = \sum(-il_a|a_i\rangle\langle a_i| - il_b|b_i\rangle\langle b_i|)$  with  $l_a$  and  $l_b$  being the losses at different sites,  $|\phi\rangle$  is the state reached,  $\tilde{\omega}$  is the excitation frequency,  $|S\rangle \equiv (0 \cdots, S_i, \cdots)^T$  represents the distribution of external sources. Here these excitation sources are all located in the linear chain, and the number of excitation sources can be reduced to one [see Fig. S7]. Given  $\tilde{\omega}$  and  $|S\rangle$ , Fig. 3(b) shows the intensity  $|\phi|^2$  of the

steady state reached at frequency  $\tilde{\omega}$  versus the amplification factor of the sources  $A$ . With the increasing of  $A$ , Fig. 3(c) shows the waveform of the corresponding excited state, which also undergoes an initial deviation from exponential decay (purple line), emerges an arbitrarily designable plateau (orange and green lines), extends to the entire nonlinear domain (blue line), and eventually diverges at the nonlinear boundary (dark cyan line). When  $l_a/v_i \ll 1$ , the corresponding waveform of the excited states in the nonlinear part can be approximated by

$$\begin{aligned} \nu_i a_i + (\tilde{\kappa}_i + \alpha a_{i+1}^2) a_{i+1} + \alpha \left( \frac{l_a}{v_i} a_i \right)^2 a_{i+1} + l_b \frac{l_a}{v_i} a_i \approx 0, \\ \text{Im}(a_i) = 0, \end{aligned} \quad (9)$$

and all  $\text{Re}(b_i) = 0$ . Since the last two terms are pretty small, the excited states and the targeted TZMs are almost identical [See Figs. 3(d) and S6]. A complementary discussion on the waveform of the excited states in the linear chain (not of interest here) is provided in the Supplemental Material, Sec. 6 [61].

These configurable excited states provide the potential for next-generation nonlinear topological devices. The stability of these excited states against noise in dynamics is critical when considering potential applications. We investigate the stability of  $|\varphi\rangle$  by adding a sudden perturbation  $|\varepsilon\rangle$  [80], and then simulating the following evolution of wave function  $|\phi\rangle = |\varphi\rangle + |\varepsilon\rangle$ . Here  $|\varepsilon\rangle$  is a uniform random noise with values inside the interval  $(-3, 3)$  and the one we used is plotted in Fig. 3(e). We implement a pretty large noise amplitude here for demonstration purposes. The effect of the disturbance can be captured by the following similarity function

$$\chi(t) = \frac{|\langle \phi(t) | \varphi \rangle|}{\sqrt{\langle \phi(t) | \phi(t) \rangle \langle \varphi | \varphi \rangle}}. \quad (10)$$

In the presence of disturbance,  $\chi(t)$  deviates from 1. Figure 3(f) shows the evolution of  $\chi$  for different  $A$  in the time domain. In a short time,  $\chi$  in all cases returns to 1. We have also checked different noise configurations, and the results are the same (see Supplemental Material, Sec. 7 [61]). Hence, the excited states are stable in dynamics, which thus exhibits potential for the applications of configurable TZMs.

**Conclusions**—In summary, we propose arbitrarily configurable TZMs by utilizing nonlinearity. Combining the inherent configurability of nonlinearity and the robustness originating from topology, the nonlinear TZMs are robust against disorders, and can be uniquely controlled by intensity. We show that with a proper excitation scheme, the system can reach a stable steady state that is almost identical to the target TZM. Our approach, free from the constraints of chiral symmetry and zero-energy modes (see Fig. S13), can be extended to higher-dimensional systems

and higher-order topological modes (see the Supplemental Material, Sec. 8 [61]) and implemented within diverse systems (see the Supplemental Material, Sec. 9 [61]), such as circuits [51,54,80], photonic waveguides [49,81], mechanical resonators [82], etc. [83,84]. Thus, we believe our findings will enrich nonlinear topological physics and provide new avenues for compact nonlinear topological devices.

**Acknowledgments**—This work is supported by the National Key Research and Development Program of China (Grant No. 2022YFA1404900), the National Natural Science Foundation of China (Grants No. 12334015, No. 12274332, No. 12274330), the China Postdoctoral Science Foundation under Grant No. 2023M742715 and Knowledge Innovation Program of Wuhan-Shuguang (Grant No. 2022010801020125).

- 
- [1] J. Wang and S.-C. Zhang, *Nat. Mater.* **16**, 1062 (2017).
  - [2] Z. Wang, Y. Chong, J. D. Joannopoulos, and M. Soljačić, *Nature (London)* **461**, 772 (2009).
  - [3] M. C. Rechtsman, J. M. Zeuner, Y. Plotnik, Y. Lumer, D. Podolsky, F. Dreisow, S. Nolte, M. Segev, and A. Szameit, *Nature (London)* **496**, 196 (2013).
  - [4] L. Lu, J. D. Joannopoulos, and M. Soljačić, *Nat. Photonics* **8**, 821 (2014).
  - [5] F. D. M. Haldane and S. Raghu, *Phys. Rev. Lett.* **100**, 013904 (2008).
  - [6] M. Hafezi, S. Mittal, J. Fan, A. Migdall, and J. M. Taylor, *Nat. Photonics* **7**, 1001 (2013).
  - [7] A. B. Khanikaev, S. Hosseini Mousavi, W.-K. Tse, M. Kargarian, A. H. MacDonald, and G. Shvets, *Nat. Mater.* **12**, 233 (2013).
  - [8] S. Mittal, S. Ganeshan, J. Fan, A. Vaezi, and M. Hafezi, *Nat. Photonics* **10**, 180 (2016).
  - [9] V. Peano, C. Brendel, M. Schmidt, and F. Marquardt, *Phys. Rev. X* **5**, 031011 (2015).
  - [10] J. Ningyuan, C. Owens, A. Sommer, D. Schuster, and J. Simon, *Phys. Rev. X* **5**, 021031 (2015).
  - [11] V. V. Albert, L. I. Glazman, and L. Jiang, *Phys. Rev. Lett.* **114**, 173902 (2015).
  - [12] S. Imhof, C. Berger, F. Bayer, J. Brehm, L. W. Molenkamp, T. Kiessling, F. Schindler, C. H. Lee, M. Greiter, T. Neupert, and R. Thomale, *Nat. Phys.* **14**, 925 (2018).
  - [13] C. H. Lee, S. Imhof, C. Berger, F. Bayer, J. Brehm, L. W. Molenkamp, T. Kiessling, and R. Thomale, *Commun. Phys.* **1**, 39 (2018).
  - [14] M. Xiao, G. Ma, Z. Yang, P. Sheng, Z. Q. Zhang, and C. T. Chan, *Nat. Phys.* **11**, 240 (2015).
  - [15] G. Ma, M. Xiao, and C. T. Chan, *Nat. Rev. Phys.* **1**, 281 (2019).
  - [16] S. D. Huber, *Nat. Phys.* **12**, 621 (2016).
  - [17] W. Wang, X. Wang, and G. Ma, *Nature (London)* **608**, 50 (2022).
  - [18] M. Hu, Y. Zhang, X. Jiang, T. Qiao, Q. Wang, S. Zhu, M. Xiao, and H. Liu, *Light Sci. Appl.* **10**, 170 (2021).
  - [19] B. Florijn, C. Coulais, and M. van Hecke, *Phys. Rev. Lett.* **113**, 175503 (2014).

- [20] Y. Hatsugai, *Phys. Rev. Lett.* **71**, 3697 (1993).
- [21] Z.-K. Lin, Q. Wang, Y. Liu, H. Xue, B. Zhang, Y. Chong, and J.-H. Jiang, *Nat. Rev. Phys.* **5**, 483 (2023).
- [22] M. Hafezi, E. A. Demler, M. D. Lukin, and J. M. Taylor, *Nat. Phys.* **7**, 907 (2011).
- [23] B. Hu, Z. Zhang, H. Zhang, L. Zheng, W. Xiong, Z. Yue, X. Wang, J. Xu, Y. Cheng, X. Liu, and J. Christensen, *Nature (London)* **597**, 655 (2021).
- [24] G. Harari, M. A. Bandres, Y. Lumer, M. C. Rechtsman, Y. D. Chong, M. Khajavikhan, D. N. Christodoulides, and M. Segev, *Science* **359**, eaar4003 (2018).
- [25] M. A. Bandres, S. Wittek, G. Harari, M. Parto, J. Ren, M. Segev, D. N. Christodoulides, and M. Khajavikhan, *Science* **359**, eaar4005 (2018).
- [26] Y. Zeng, U. Chattopadhyay, B. Zhu, B. Qiang, J. Li, Y. Jin, L. Li, A. G. Davies, E. H. Linfield, B. Zhang, Y. Chong, and Q. J. Wang, *Nature (London)* **578**, 246 (2020).
- [27] S. Barik, A. Karasahin, C. Flower, T. Cai, H. Miyake, W. DeGottardi, M. Hafezi, and E. Waks, *Science* **359**, 666 (2018).
- [28] A. Blanco-Redondo, B. Bell, D. Oren, B. J. Eggleton, and M. Segev, *Science* **362**, 568 (2018).
- [29] S. Mittal, E. A. Goldschmidt, and M. Hafezi, *Nature (London)* **561**, 502 (2018).
- [30] S. Yao and Z. Wang, *Phys. Rev. Lett.* **121**, 086803 (2018).
- [31] A. McDonald, T. Pereg-Barnea, and A. A. Clerk, *Phys. Rev. X* **8**, 041031 (2018).
- [32] F. K. Kunst, E. Edvardsson, J. C. Budich, and E. J. Bergholtz, *Phys. Rev. Lett.* **121**, 026808 (2018).
- [33] N. Hatano and D. R. Nelson, *Phys. Rev. Lett.* **77**, 570 (1996).
- [34] S. Longhi, D. Gatti, and G. D. Valle, *Sci. Rep.* **5**, 13376 (2015).
- [35] W. Zhu, W. X. Teo, L. Li, and J. Gong, *Phys. Rev. B* **103**, 195414 (2021).
- [36] S. Longhi, *Ann. Phys. (Berlin)* **530**, 1800023 (2018).
- [37] S. Wong and S. S. Oh, *Phys. Rev. Res.* **3**, 033042 (2021).
- [38] V. V. Konotop, J. Yang, and D. A. Zezyulin, *Rev. Mod. Phys.* **88**, 035002 (2016).
- [39] D. Smirnova, D. Leykam, Y. Chong, and Y. Kivshar, *Appl. Phys. Rev.* **7**, 021306 (2020).
- [40] K. Bai, L. Fang, T.-R. Liu, J.-Z. Li, D. Wan, and M. Xiao, *Natl. Sci. Rev.* **10**, nwac259 (2022).
- [41] K. Bai, J.-Z. Li, T.-R. Liu, L. Fang, D. Wan, and M. Xiao, *Phys. Rev. Lett.* **130**, 266901 (2023).
- [42] S. Assaworrorarit, X. Yu, and S. Fan, *Nature (London)* **546**, 387 (2017).
- [43] P.-W. Lo, C. D. Santangelo, B. Bryan Gin-ge Chen, C.-M. Jian, K. Roychowdhury, and M. J. Lawler, *Phys. Rev. Lett.* **127**, 076802 (2021).
- [44] S. Xia, D. Jukić, N. Wang, D. Smirnova, L. Smirnov, L. Tang, D. Song, A. Szameit, D. Leykam, J. Xu, Z. Chen, and H. Buljan, *Light Sci. Appl.* **9**, 147 (2020).
- [45] Z. Hu, D. Bongiovanni, D. Jukić, E. Jajtić, S. Xia, D. Song, J. Xu, R. Morandotti, H. Buljan, and Z. Chen, *Light Sci. Appl.* **10**, 164 (2021).
- [46] D. Leykam and Y. D. Chong, *Phys. Rev. Lett.* **117**, 143901 (2016).
- [47] S. Mukherjee and M. C. Rechtsman, *Phys. Rev. X* **11**, 041057 (2021).
- [48] Y. Lumer, Y. Plotnik, M. C. Rechtsman, and M. Segev, *Phys. Rev. Lett.* **111**, 243905 (2013).
- [49] S. Mukherjee and M. C. Rechtsman, *Science* **368**, 856 (2020).
- [50] Y. Hadad, A. B. Khanikaev, and A. Alù, *Phys. Rev. B* **93**, 155112 (2016).
- [51] Y. Hadad, J. C. Soric, A. B. Khanikaev, and A. Alù, *Nat. Electron.* **1**, 178 (2018).
- [52] L. J. Maczewsky, M. Heinrich, M. Kremer, S. K. Ivanov, M. Ehrhardt, F. Martinez, Y. V. Kartashov, V. V. Konotop, L. Torner, D. Bauer, and A. Szameit, *Science* **370**, 701 (2020).
- [53] M. S. Kirsch, Y. Zhang, M. Kremer, L. J. Maczewsky, S. K. Ivanov, Y. V. Kartashov, L. Torner, D. Bauer, A. Szameit, and M. Heinrich, *Nat. Phys.* **17**, 995 (2021).
- [54] F. Zangeneh-Nejad and R. Fleury, *Phys. Rev. Lett.* **123**, 053902 (2019).
- [55] S. Xia, D. Kaltsas, D. Song, I. Komis, J. Xu, A. Szameit, H. Buljan, K. G. Makris, and Z. Chen, *Science* **372**, 72 (2021).
- [56] T. Dai, Y. Ao, J. Mao, Y. Yang, Y. Zheng, C. Zhai, Y. Li, J. Yuan, B. Tang, Z. Li, J. Luo, W. Wang, X. Hu, Q. Gong, and J. Wang, *Nat. Phys.* **20**, 101 (2024).
- [57] S. Wong, T. A. Loring, and A. Cerjan, *Phys. Rev. B* **108**, 195142 (2023).
- [58] W. Cheng, A. Cerjan, S.-Y. Chen, E. Prodan, T. A. Loring, and C. Prodan, *Nat. Commun.* **14**, 3071 (2023).
- [59] K. Y. Dixon, T. A. Loring, and A. Cerjan, *Phys. Rev. Lett.* **131**, 213801 (2023).
- [60] W. P. Su, J. R. Schrieffer, and A. J. Heeger, *Phys. Rev. Lett.* **42**, 1698 (1979).
- [61] See Supplemental Material at <http://link.aps.org/supplemental/10.1103/PhysRevLett.133.116602>, which includes [24,25,30,40,42,46–54,58,62–76], for further details.
- [62] S. Kruk, A. Poddubny, D. Smirnova, L. Wang, A. Slobozhanyuk, A. Shorokhov, I. Kravchenko, B. Luther-Davies, and Y. Kivshar, *Nat. Nanotechnol.* **14**, 126 (2019).
- [63] S. Wong, T. A. Loring, and A. Cerjan, *Phys. Rev. B* **108**, 195142 (2023).
- [64] A. Cerjan, T. A. Loring, and F. Vides, *J. Math. Phys. (N.Y.)* **64**, 023501 (2023).
- [65] T. A. Loring, *Ann. Phys. (Amsterdam)* **356**, 383 (2015).
- [66] A. Cerjan and T. A. Loring, *Phys. Rev. B* **106**, 064109 (2022).
- [67] T. Loring and H. Schulz-Baldes, *J. Noncommut. Geom.* **14**, 1 (2018).
- [68] T.-R. Liu, K. Bai, J.-Z. Li, L. Fang, D. Wan, and M. Xiao, *Phys. Rev. B* **108**, L081101 (2023).
- [69] D. Zhou, D. Z. Rocklin, M. Leamy, and Y. Yao, *Nat. Commun.* **13**, 3379 (2022).
- [70] B. Xie, H.-X. Wang, X. Zhang, P. Zhan, J.-H. Jiang, M. Lu, and Y. Chen, *Nat. Rev. Phys.* **3**, 520 (2021).
- [71] W. A. Benalcazar, B. A. Bernevig, and T. L. Hughes, *Science* **357**, 61 (2017).
- [72] M. J. Rice and E. J. Mele, *Phys. Rev. Lett.* **49**, 1455 (1982).
- [73] D. Leykam, S. Mittal, M. Hafezi, and Y. D. Chong, *Phys. Rev. Lett.* **121**, 023901 (2018).
- [74] X. Guo, L. Jezequel, M. Padlewski, H. Lissek, P. Delplace, and R. Fleury, [arXiv:2403.10590](https://arxiv.org/abs/2403.10590).
- [75] C. Wang, J. Rao, Z. Chen, K. Zhao, L. Sun, B. Yao, T. Yu, Y.-P. Wang, and W. Lu, *Nat. Phys.* **20**, 1139 (2024).

- [76] Z.-X. Chen, Y.-g. Peng, Z.-G. Chen, Y. Liu, P. Chen, X.-f. Zhu, and Y.-q. Lu, *Nat. Commun.* **15**, 1478 (2024).
- [77] M.D. Caio, G. Möller, N.R. Cooper, and M.J. Bhaseen, *Nat. Phys.* **15**, 257 (2019).
- [78] J. Sykes and R. Barnett, *Phys. Rev. B* **103**, 155134 (2021).
- [79] J.D. Hannukainen, M.F. Martínez, J.H. Bardarson, and T.K. Kivornig, *Phys. Rev. Lett.* **129**, 277601 (2022).
- [80] D. Zhou, D.Z. Rocklin, M. Leamy, and Y. Yao, *Nat. Commun.* **13**, 3379 (2022).
- [81] S. Mittal, G. Moille, K. Srinivasan, Y.K. Chembo, and M. Hafezi, *Nat. Phys.* **17**, 1169 (2021).
- [82] L. Papariello, O. Zilberberg, A. Eichler, and R. Chitra, *Phys. Rev. E* **94**, 022201 (2016).
- [83] Y.-P. Wang, G.-Q. Zhang, D. Zhang, T.-F. Li, C.-M. Hu, and J. Q. You, *Phys. Rev. Lett.* **120**, 057202 (2018).
- [84] N. Pernet, P. St-Jean, D.D. Solnyshkov, G. Malpuech, N. Carlon Zambon, Q. Fontaine, B. Real, O. Jamadi, A. Lemaître, M. Morassi, L. Le Gratiet, T. Baptiste, A. Harouri, I. Sagnes, A. Amo, S. Ravets, and J. Bloch, *Nat. Phys.* **18**, 678 (2022).